Electronic Supplementary Material (ESI) for Journal of Materials Chemistry B.

Supporting Information

An Injectable Polypeptide-engineered Hydrogel Depot for Amplifying Anti-tumor Immune Effect Induced by Chemo-photothermal Therapy

*Xiao-lin Hou,[a,1] Xiang Dai,[b,1] Jie Yang,[a] Bin Zhang,[a] Dong-hui Zhao,[a] Chao-qing Li,[a] Zhong-yuan Yin,[*c] Yuan-di Zhao,[a,d] and Bo Liu[*a]*

[a] Britton Chance Center for Biomedical Photonics at Wuhan National Laboratory for Optoelectronics-Hubei Bioinformatics & Molecular Imaging Key Laboratory, Department of Biomedical Engineering, College of Life Science and Technology, Huazhong University of Science and Technology, Wuhan 430074, Hubei, P. R. China

[b] Eugenic Genetics Laboratory, Wuhan Children's Hospital (Wuhan Maternal and Child Healthcare Hospital), Tongji Medical College, Huazhong University of Science & Technology, Wuhan 430074, Hubei, P. R. China

[c] Cancer center, Union Hospital, Tongji Medical College, Huazhong University of Science and Technology, Wuhan 430022, Hubei, P. R. China.

[d] Key Laboratory of Biomedical Photonics (HUST), Ministry of Education, Huazhong University of Science and Technology, Wuhan 430074, Hubei, P. R. China

* Corresponding author.

Fax: (+) 86 27-8779-2202

E-mail address: yzyunion@163.com (Z.-Y. Yin); lbyang@mail.hust.edu.cn (B. Liu)

[1] These authors contributed equally to this work

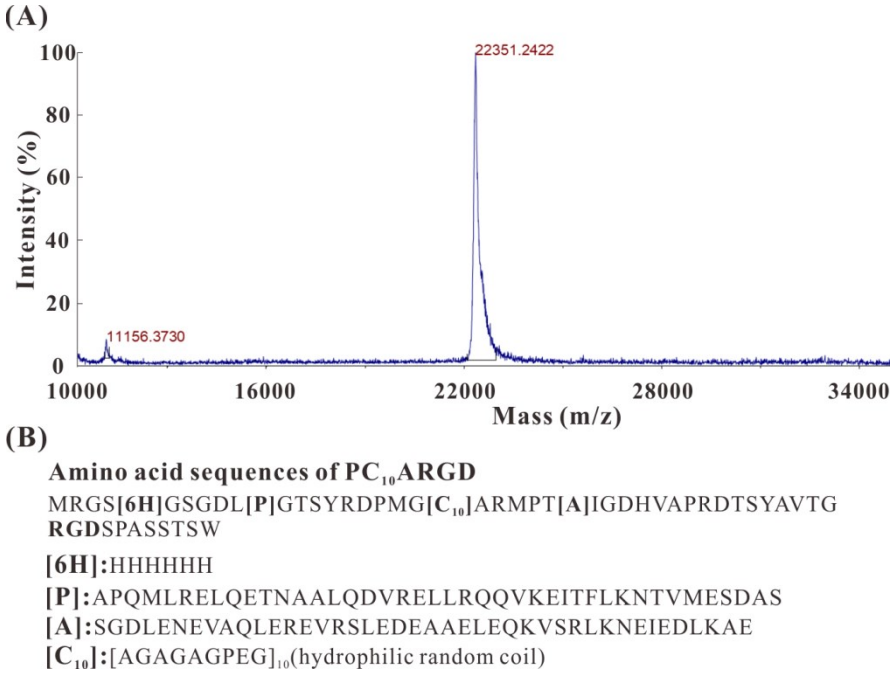

Figure S1. (A) Amino acid sequences and B) mass spectrum of $PC_{10}ARGD$ polypeptide.

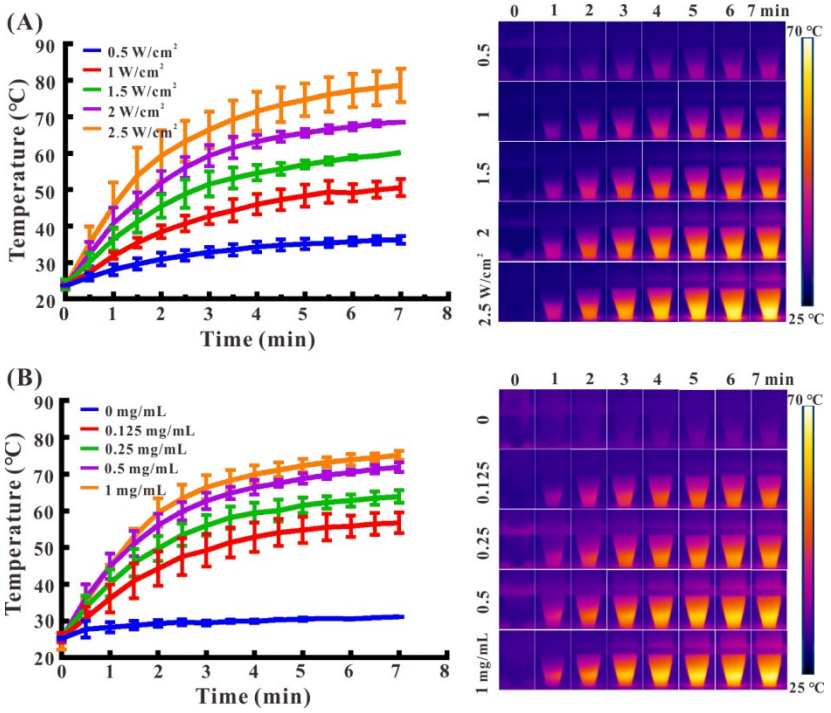

Figure S2. (A) Heating curves and infrared thermal images of Ag_2S QD@$PC_{10}ARGD$ nanogel at different powers (0.5 mg mL^{-1} Ag ions, laser intensity from 0.5 to 2.5 W cm^{-2}) and (B) various concentrations (laser intensity: 2 W cm^{-2}, Ag ions from 0 to 1 mg mL^{-1})

under exposure to an 808 nm laser.

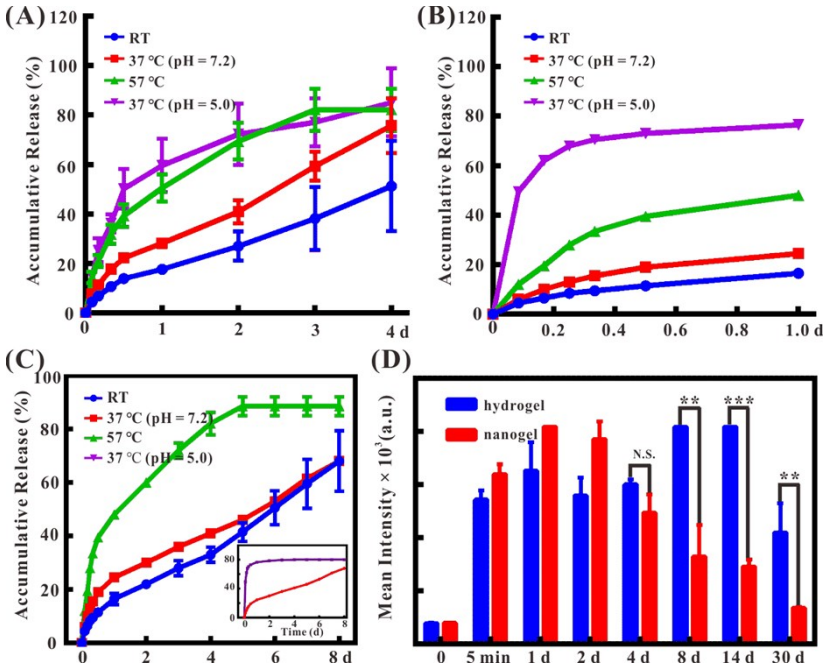

Figure S3. (A) *In vitro* Bestatin release profile from hydrogel under differernt conditions and (B) short-term DOX release from DOX@PC_{10}ARGD hydrogels under various conditions. (C) *In vitro* DOX release profile from DOX@PC10ARGD hydrogels under different conditions in vitro and (D) mean intensityof injection sites detected through near-infrared fluorescence of Ag_2S QD. The data are expressed as the means ± SD (n=3). Statistical analysis was performed by Student's t-test. ** P<0.01, *** P<0.001, N.S. = not statistically significant difference.

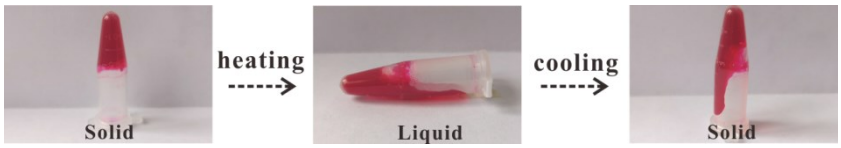

Figure S4. Phase transition of R-6G@PC_{10}ARGD hydrogel (solid-liquid-solid).

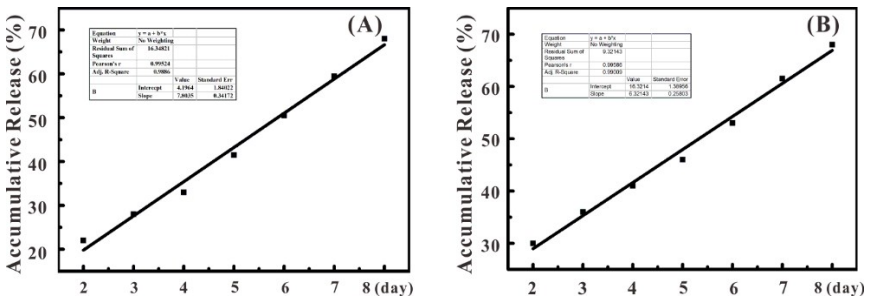

Figure S5. *In vitro* DOX linear release profile of DOX@PC_{10}ARGD hydrogel (from day 2 to 8) at A) RT and B) 37 ℃ (pH = 7.2).

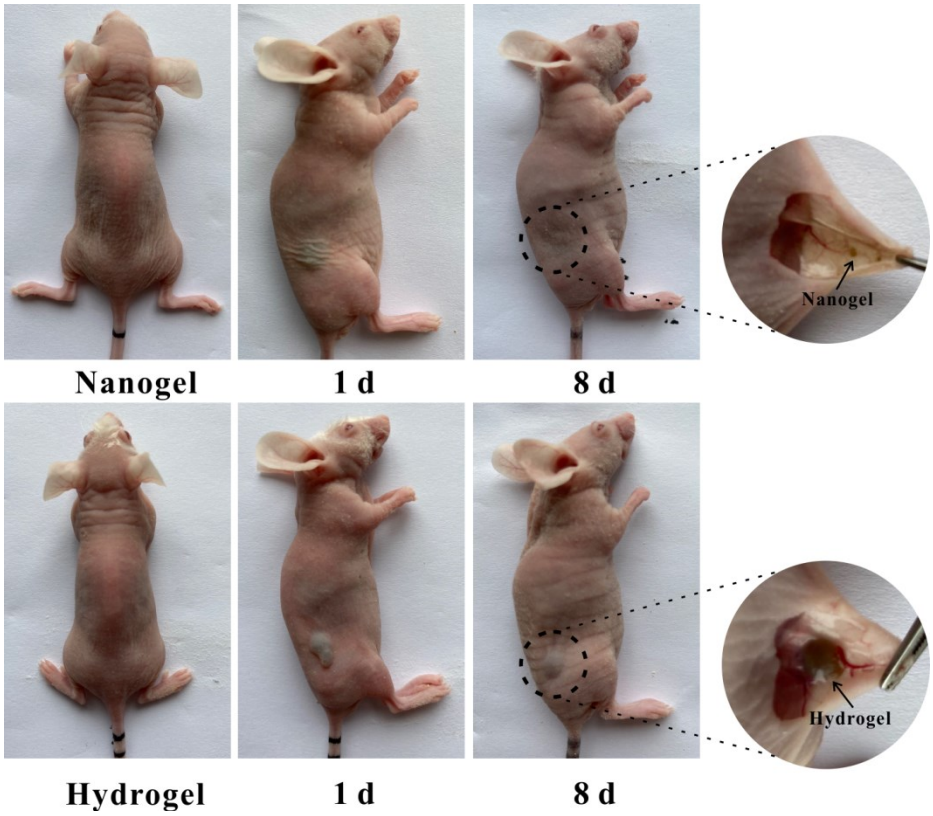

Figure S6. The degradation effects of nanogels and hydrogels *in vivo*.

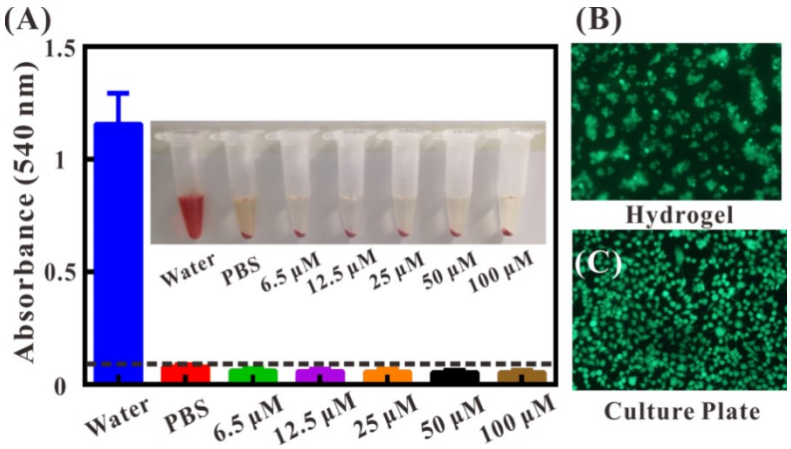

Figure S7. (A) Hemolysis effects on RBCs of PC_{10}ARGD solutions with different concentrations (from 0 to 100 μM). (B, C) *In vitro* 4T1 cells were cultured with culture plates with/without PC_{10}ARGD hydrogel, Live and dead cells were stained with calcein-AM (green) and PI (red).

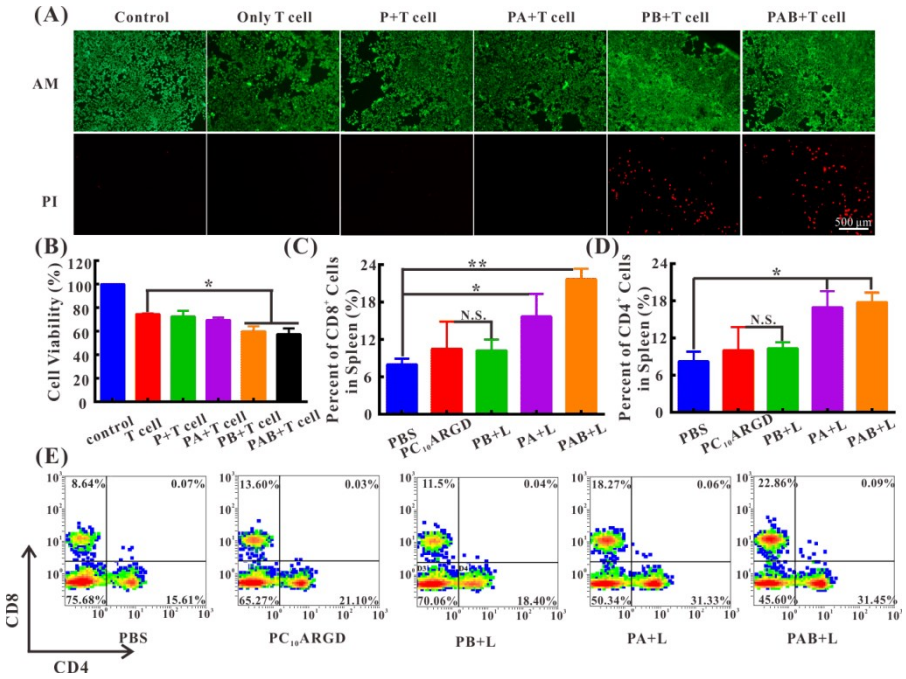

Figure S8. *In vitro* and *in vivo* immune response after treating with various hydrogels. (A) Fluorescence images of 4T1 cells after co-cultured with DCs, T cells, and different hydrogels. 4T1 cells were pre-treated with AM (green) and PI (red). (B) Immune-cytotoxicity of T lymphocytes to 4T1 tumor cells using MTT assay. (E) Representative flow cytometry plots

showing $CD8^+$ T cells and $CD4^+$ T cells, and (C, D) the percentage of $CD8^+$ and $CD4^+$ cells in the spleen cells after various treatments. Statistical analysis was performed by Student's t-test. * $P<0.05$, ** $P<0.01$, N.S. = not statistically significant difference.

It has been reported that many ablative tumor treatments such as PTT, photodynamic therapy, and chemotherapy can induce tumor-specific immune response [1]. However, the tumor has formed TMEs during growth, and it is difficult to provide an effective immune effect on the basis of chemo-photothermal therapy alone. Therefore, an immune-adjunct drug Bestatin was integrated into PC_{10}ARGD hydrogel. To demonstrate the killing ability of immune response *in vitro*, a triple-cell co-cultured model of T lymphocytes/DCs/4T1 cells (50:10:1) was established. As DCs serve as master regulators of T-cell adaptive immunity, the bone marrow-derived dendritic cells (BMDCs) were harvested from femurs and tibiae of C57BL/6 mouse. In order to imitate the process of TAAs released from dying cells, 4T1 cells were put into -80 ℃ and froze repeatedly to obtain TAAs. The triple-cell co-cultured model incubated with various hydrogels and treated with the obtained TAAs. After treatment for 48 h, the tumor cells were stained with AM/PI, and the alive/dead was observed by fluorescence microscope. Both PB and PAB group were obvious observed the PI signal, indicating that Bestatin in the hydrogel could release from hydrogel to elevate the killing performance of T cells (Figure S7A). The results of MTT assay revealed that the tumor inhibition rate of PB and PAB group were 40% and 42.5%, respectively, also exhibiting that Bestatin in the hydrogel could promote the killing effect of T lymphocytes (Figure S7B, $P<0.05$).

On the basis of the experimental results *in vitro*, we further examined the effects of PTT and immunotherapy on anti-tumor T-cell immunity *in vivo*. Balb/c mice were inoculated with 4T1 cells

and treated with 50 μL different hydrogels by intratumoral injection, and irradiated by an 808 nm laser at the density of 2 W cm^{-2} for 7 min. The temperature of the tumor site was monitored by a near-infrared camera. Obviously, the temperature of PA+L and PAB+L groups quickly reached 57 ℃ (Figure S8A), which was enough to effectively ablate tumors [2]. In contrast, the temperature of mice treated with PBS, $PC_{10}ARGD$, and PB increased slightly (Figure S8B). After treating with PTT three days, mice were euthanized, and splenocyte-derived T cells were collected for assessment by flow cytometry after co-staining with CD4-FITC and CD8a-PE antibody. The proportion of $CD8^+$ cells induced by the PA and the PAB hydrogel group were 18.27% and 22.86%, respectively (Figure S7E), which were 2.1 times and 2.64 times higher than those of the control groups, respectively (Figure S7C). T helper cells ($CD4^+$ cells) were also significantly increased in PAB+L group compared with the control group (Figure S7D, $p<0.05$). These results indicated that PTT induces immune effects and Bestatin could amplify the photothermal-induced immunotherapy effects. Interestingly, no obvious increasing of T cells in the PB group was observed. It is possible that no TAAs was released from the tumor sites without laser irradiation, resulting in the inability of DCs to provoke T lymphocytes.

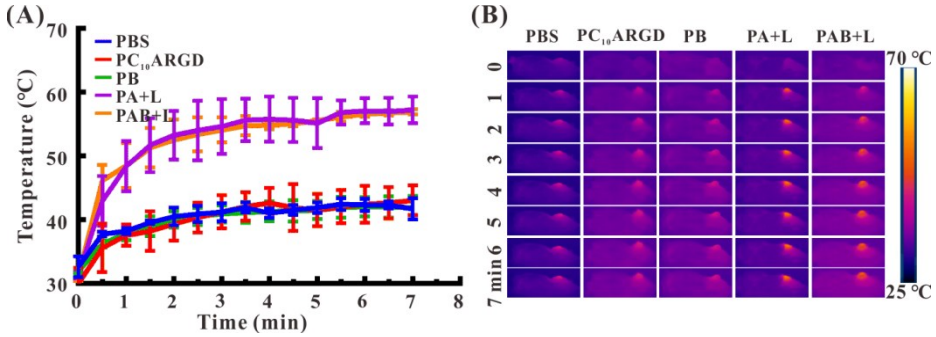

Figure S9. (A) Temperature change and B) infrared thermal images of tumors by intratumoral injection with PBS, $PC_{10}ARGD$, PB, PA, and PAB hydrogel and irradiation with an 808 nm laser at 2 w cm^{-2}.

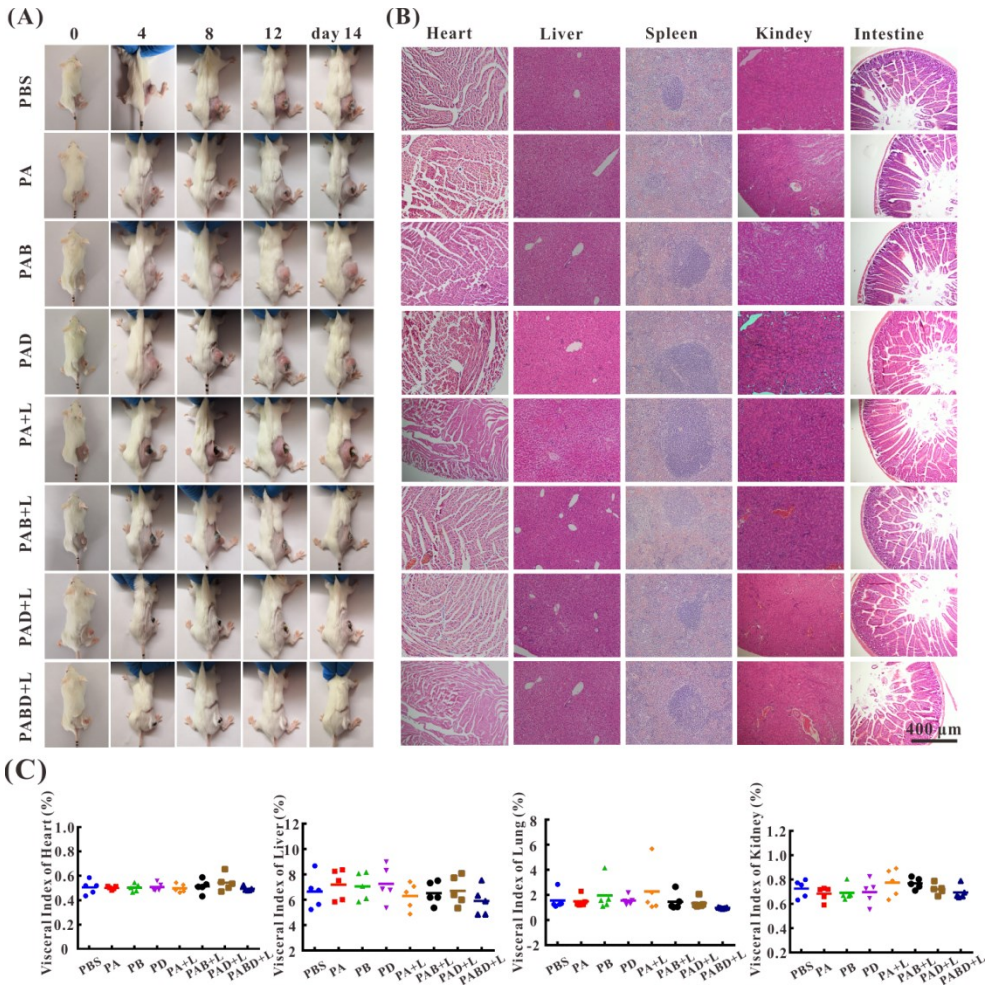

Figure S10. (A) Photographs of tumor-bearing mice and (B) H&E staining of major organs after treatment for 14 days. (C) Visceral index of major organs after different treatments.

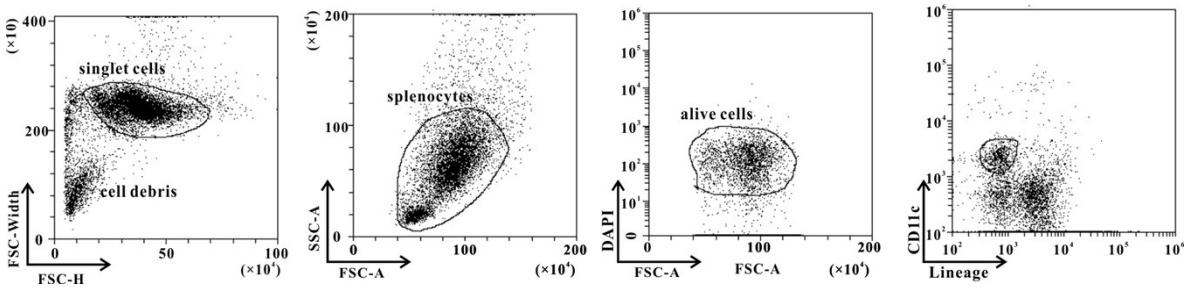

Figure S11. (A) Gating strategy for assessment the maturation of DCs (lineage$^-$CD11c$^+$) in spleen.

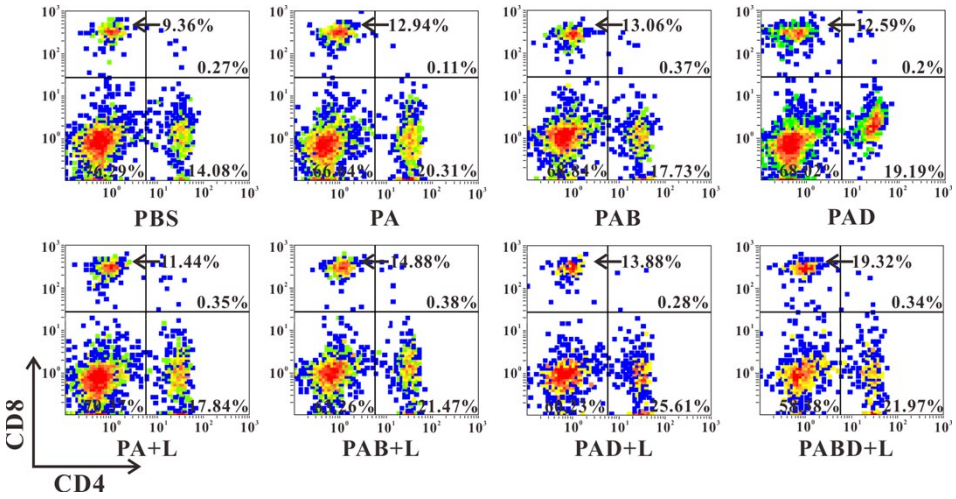

Figure S12. The percentage of CD8$^+$ and CD4$^+$ T cells in the spleen cells after various treatments

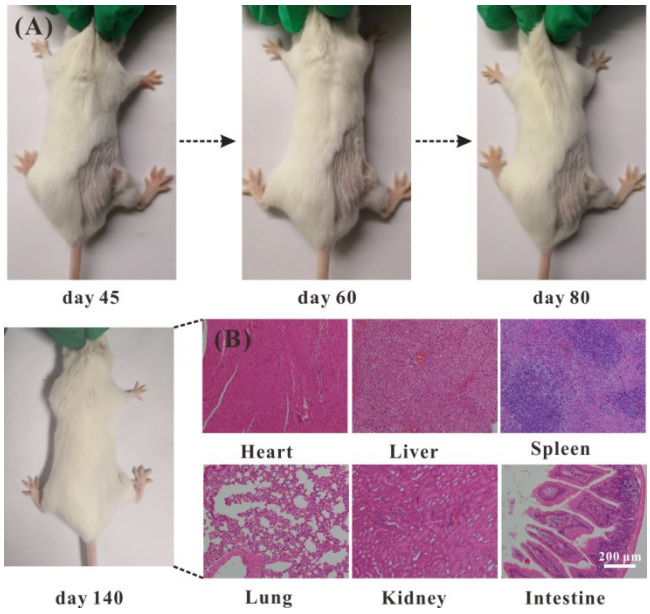

Figure S13. (A) Photographs of mouse and (B) the H&E staining of major organs after treatment for 140 days.

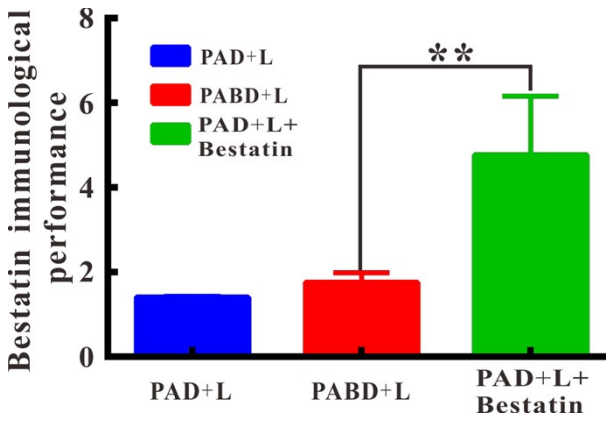

Figure S14. Anti-tumor immunological performance of Bestatin after different treatments *in vivo*. Statistical analysis was performed by Student's t-test. ** P<0.01.

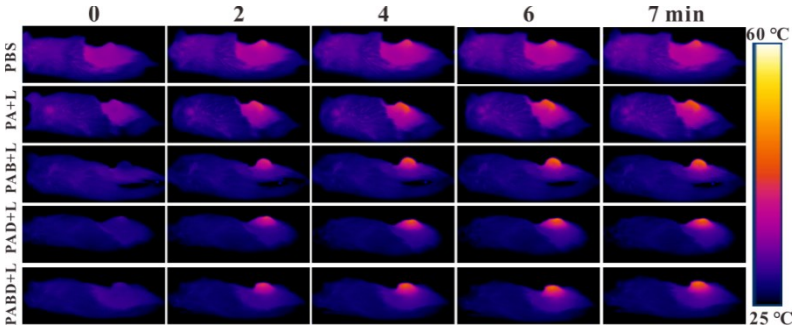

Figure S15. Infrared thermal images of 4T1-tumor-bearing mice by intratumorally injected with 50 μL various hydrogels and irradiated with an 808 nm laser at 1 W cm^{-2}.

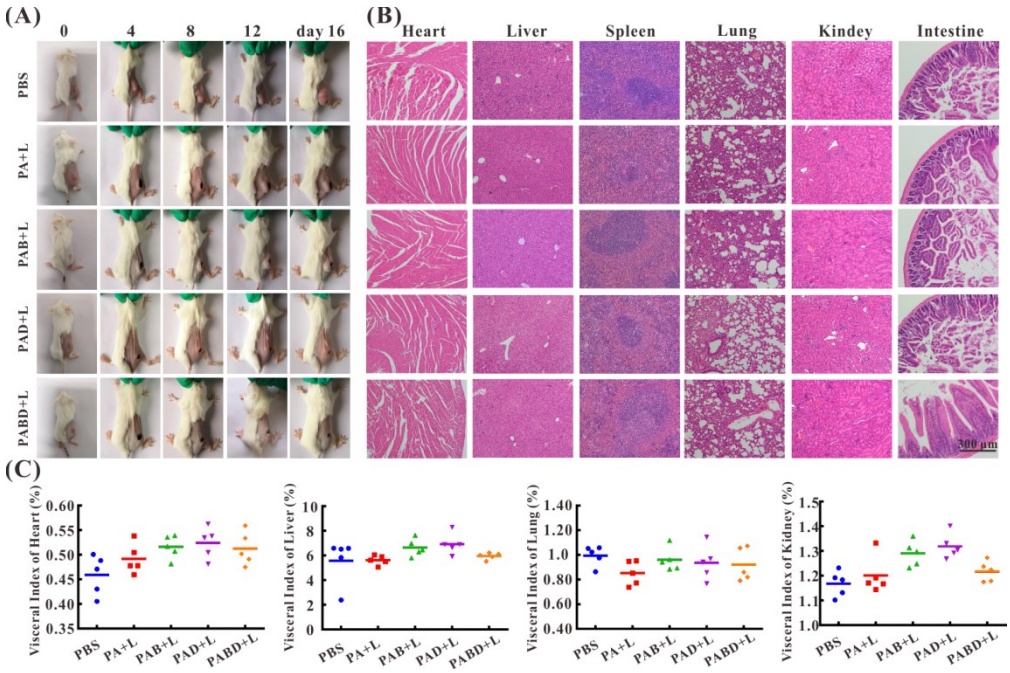

Figure S16. (A) Photographs of tumor-bearing mice and (B) H&E staining of major organs after treatment for 16 days. (C) Visceral index of major organs after treated with different hydrogels.

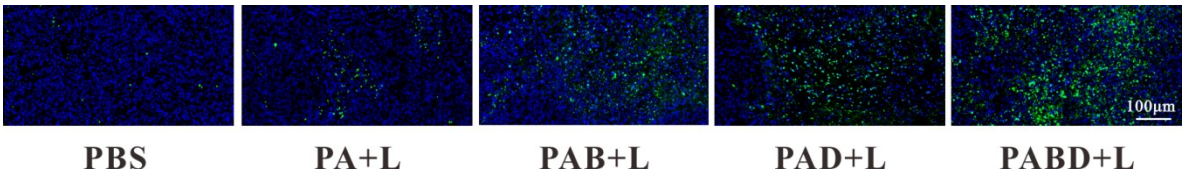

Figure S17. Representative images of tumors after TUNEL immunofluorescent staining

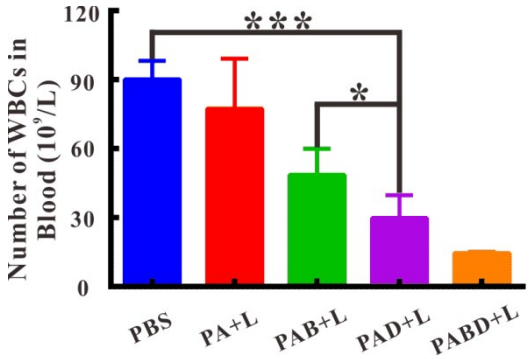

Figure S18. The number of WBCs in blood with different treatments by blood routine examination. $^{*}P<0.05$, $^{***}P<0.001$

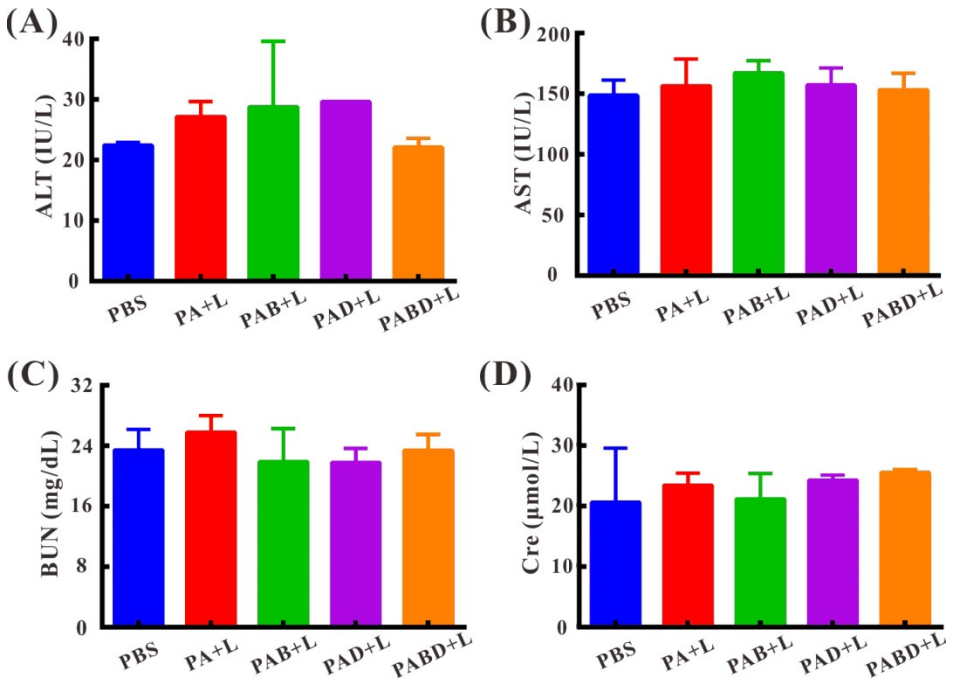

Figure S19. Serum biochemical analysis in different groups at the end of treatments (n = 3).

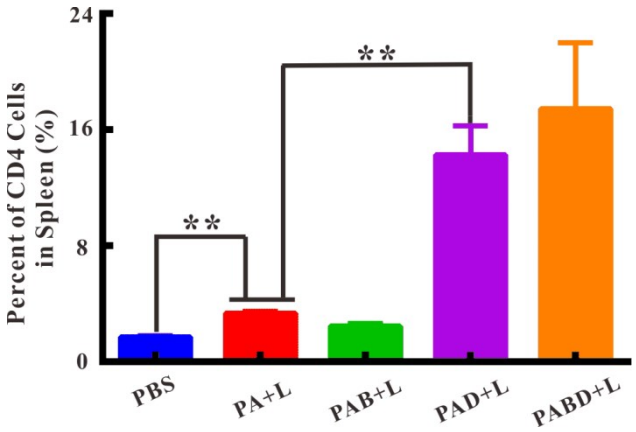

Figure S20. Activated $CD4^+$ T lymphocytes ratio in spleen of mice treated with different hydrogels.

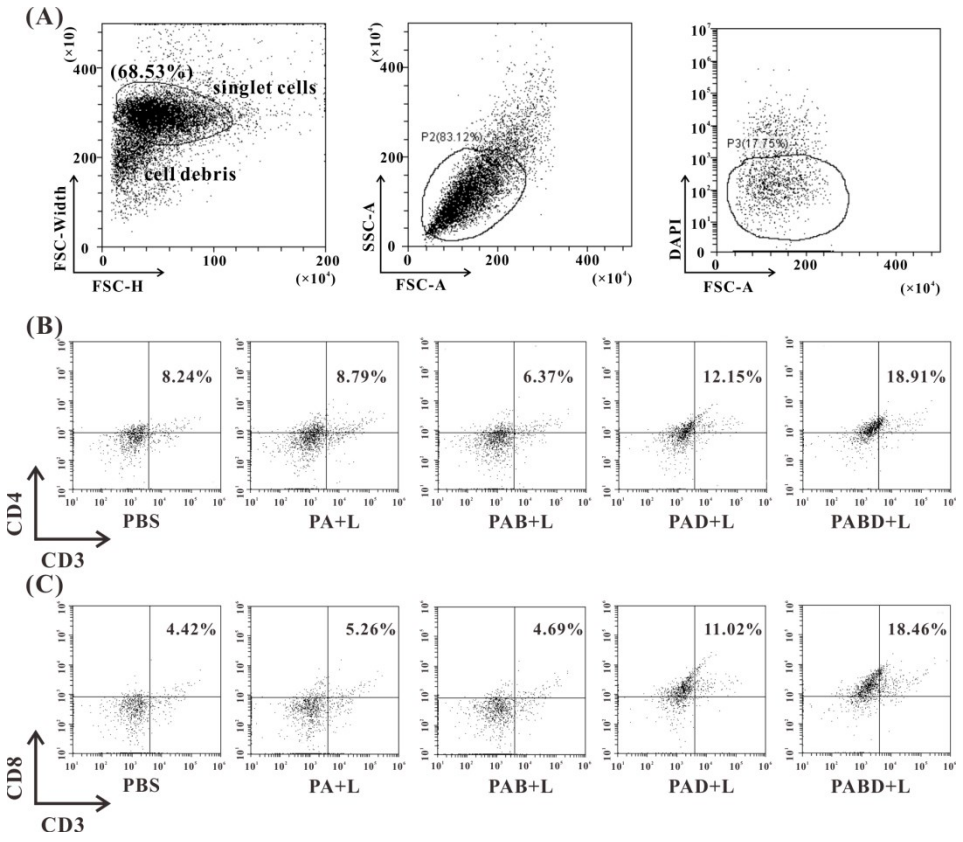

Figure S21. Activation of immune responses in tumor microenvironment. (A) Gating strategy for assessment the maturation of T cells (gated on $CD3^+$) in spleen. Representative flow cytometry plots of (B) $CD4^+$ T cells and (C) CD8 T cells.

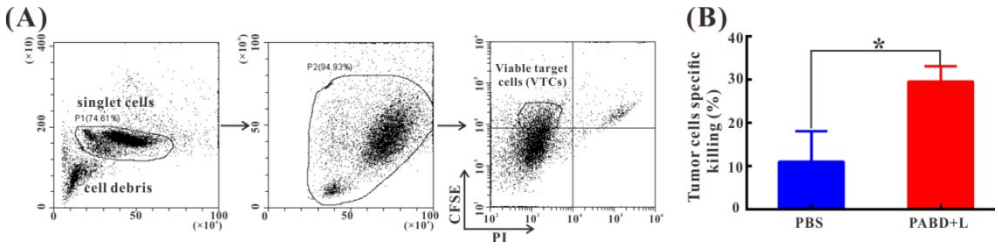

Figure S22. (A) Gating strategy for assessment cancer antigen-specific immune activation. (B) Percentage cytotoxicity specific for cancer antigen. Statistical analysis was performed by Student's t-test. *P<0.05.

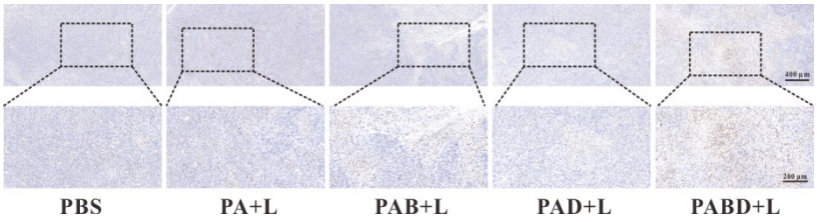

Figure S23. The infiltration of immune cells was evaluated by immunochemical staining of CD45 after various hydrogels plus laser irradiation treatment.

References

(1) Q. Chen, Q. Hu, E. Dukhovlinova, G. Chen, S. Ahn, C. Wang, E. A. Ogunnaike, F. S. Ligler, G. Dotti, Z. Gu, *Adv. Mater.,* 2019, **31**, 1900192.

(2) L. R. Guo, D. D. Yan, D. F. Yang, Y. J. Li, X. D. Wang, O. Zalewski, B. F. Yan, W. Lu, *ACS Nano,* 2014, **8**, 5670-5681.